Mon. Not. R. Astron. Soc. **000**, 000–000 (0000) Printed 29 March 2011 (MN LATEX style file v2.2)

The Local Bias Model in the Large Scale Halo Distribution

M.Manera[1,2] & E.Gaztañaga[3]
[1] *Institute of Cosmology and Gravitation, University of Portsmouth, Dennis Sciama Building, Burnaby Road, Portsmouth PO1 3FX, UK*
[2] *Center for Cosmology and Particle Physics, New York University, 4 Washington Place, NY 1003, New York,USA*
[3] *Institut de Ciències de l'Espai, CSIC/IEEC, Campus UAB, F. de Ciències, Torre C5 par-2, Barcelona 08193, Spain*

arXiv:0912.0446v4 [astro-ph.CO] 28 Mar 2011

29 March 2011

ABSTRACT

We explore the biasing in the clustering statistics of halos as compared to dark matter (DM) in simulations. We look at the second and third order statistics at large scales of the (intermediate) MICEL1536 simulation and also measure directly the local bias relation $h = f(\delta)$ between DM fluctuations, δ, smoothed over a top-hat radius R_s at a point in the simulation and its corresponding tracer h (i.e. halos) at the same point. This local relation can be Taylor expanded to define a linear (b_1) and non-linear (b_2) bias parameters. The values of b_1 and b_2 in the simulation vary with R_s approaching a constant value around $R_s > 30-60$ Mpc/h. We use the local relation to predict the clustering of the tracer in terms of the one of DM. This prediction works very well (about percent level) for the halo 2-point correlation $\xi(r_{12})$ for $r_{12} > 15$ Mpc/h, but only when we use the biasing values that we found at very large smoothing radius $R_s > 30-60$ Mpc/h. We find no effect from stochastic or next to leading order terms in the $f(\delta)$ expansion. But we do find some discrepancies in the 3-point function that needs further understanding. We also look at the clustering of the smoothed moments, the variance and skewness which are volume average correlations and therefore include clustering from smaller scales. In this case, we find that both next to leading order and discreetness corrections (to the local model) are needed at the $10-20\%$ level. Shot-noise can be corrected with a term $\sigma_e^2/\bar{n}$ where $\sigma_e^2 < 1$, i.e., always smaller than the Poisson correction. We also compare these results with the peak-background split predictions from the measured halo mass function. We find 5-10% systematic (and similar statistical) errors in the mass estimation when we use the halo model biasing predictions to calibrate the mass.

1 INTRODUCTION

To do precision cosmology it is important to understand accurately galaxy bias, i.e., how the spatial distribution of galaxies is related to the underlying dark matter distribution. Because galaxies are known to form in dark matter halos, its biasing can be approached in two natural steps. The first step is the bias between halos and dark matter. The second step is the bias between galaxies and halos, which is commonly approached by means of models of galaxy occupation in halos (see for instance Zheng et al 2005 & 2009, Brown 2008, Tinker 2006 & 2010).

Biasing requires a complex modeling and in this paper we will focus on the first step only. This means that our findings might not be directly applicable to galaxy surveys. In the limit in which halo biasing resembles galaxy biasing or in the limit where observations are good tracers of the halo distribution (i.e., for galaxy groups or clusters) our results will be of direct relevance to the interpretation of clustering statistics in galaxy and cluster surveys.

We will study the halo bias in a big cosmological dark matter simulation from the MICE collaboration (Fosalba et al. 2008, Crocce et al. 2009). [1]. We will address two main questions: a) how accurate is the so-called *local* bias model to predict clustering statistics, and b) how bias predictions from the mass function compare with the ones in local model. In the process of answering these questions we will also learn about nonlinear and stochasticity contributions to the halo variance. The local bias model, introduced by Fry and Gaztañaga (1993), assumes a general non-linear (but local and deterministic) relation between the smoothed density contrast in the distribution of halos (or galaxies) and the smoothed density contrast of the dark matter, i.e., $\delta_h = F[\delta_m]$. In reality, bias is stochastic and not quite deterministic (eg., see Somerville et al. 1999, Tegmark & Bomley 1999, Dekel & Lahav 1999) and at some level, due to tidal forces and evolution, it will have non-local and anisotropic

[1] For more information about the MICE collaboration team and the simulations, see http://ice.cat.es/mice/

© 0000 RAS

contributions. It is also not clear to what extent the halo or galaxy density should depend only on the underlying matter density, without including other direct dependencies (like the gravitational potential or velocity fields, for instance). Bias could also relate to mass at some initial condition or in Lagrangian space (see, Catelan, Matarrese & Porciani 1998, Matsubara 2008 and references therein).

The bias parameters of the local model are the coefficients of the Taylor expansion of $F[\delta]$, and depend on the halo and dark matter smoothing scale. In this paper we show that for halo samples with a minimum mass less than 10^{14} solar masses the bias parameters converge at a smoothing scale $\sim$ 30-60 Mpc/h. We can then compare these local bias parameters obtained by directly fitting $F[\delta]$ in the simulations with the bias from clustering measurements like the two and 3-point correlations functions, the variance and the skewness. We will show that the local bias model works well at least within a few percent level. When this local model is applied to interpret real galaxy surveys it can be used to recover information about dark matter clustering and biasing parameters.

One common way to predict the bias parameters is to use the peak background split Ansatz. Bias parameters are predicted from the mass function using few assumptions: locality and also the assumption that the conditional mass function of an overdense (underdense) patch of the universe can be treated as if it were equal to the average mass function of the universe at a different time, or mean density. Peak background split predictions for the bias, specially from the Sheth Tormen mass function (Sheth and Tormen 1999), and the Press-Schechter mass function (Press & Schechter 1974, PS from now on) have been used a lot in the literature. In the second part of this paper we will compare these bias predictions with the bias from clustering, and with the local bias, and study their dependence on the halo mass threshold used to fit the mass function. The inaccuracy of the peak background split has also been studied in Manera, Sheth and Scoccimarro (2010) with complementary results to those of this work.

The peak background split bias parameters predicted from the Press-Schechter (PS) mass function *together* with the assumption of the local bias was tested in a precursor paper by Mo, Jing and White (1997), where the local model was used to compare the skewness and higher order moments of halos in N-Body simulations with predictions and observations, leading to the conclusion that the galaxies from the APM survey (as measured in Gaztanaga 1994) should not be highly biased. Mo, Jing and White used a small simulation of only 256 Mpc/h and 128^3 particles with plots that show no errorbars. In some of their plots, specially when halos are identified at the same time that moments are calculated, differences between theory and simulations could be interpreted as being significant for our current precision requirements. Unfortunately since they tested the PS bias parameters and the local bias model together, it is unclear how each assumption contributes to the mismatch.

In a follow-up paper, Casas-Miranda, Mo and Boener (2003) redid the previous analysis, this time with the Sheth and Tormen mass function, and applied the results to the Lyman break galaxies at $z = 3$. Their plots of skewness and higher order moments still show no error bars, and differences between theory and simulations could amount more than 15% in some cases. Again, the question arises to whether the local bias is a good approximation or not independent of the bias prediction from the mass function, which requires extra assumptions and varies depending which mass function one decides to use. In our paper we can separate these effects by obtaining the local bias parameters directly from a fit of the local bias relation F, thus testing the local model separately, from the bias predictions. A failure of the local bias model could point towards what other contributions should be included next (if any) when analysing observational data to the precision needed for the current generation of surveys.

Another difference in our analysis with respect to the previous works above is that we study both moments (variance and skewness) and 2 and 3-point correlation functions. Moments are closer to the local relation in that they are both smoothed (spherically averaged) quantities, so one would expect better agreement for them. But they suffer from shot-noise (or discreteness effects) and stronger non-linear effects (as they include clustering on all scales smaller than the smoothing radius). The 2 and 3-point functions do not suffer from shot-noise and can better separate the effect of different scales (because they are averaged over radial shells rather than integrated over spheres). Moreover, the 3-point function provides different information than the skewness. Both are related third order statistics, but the 3-point function also gives shape information (i.e., how elongated are the triangles) which is missing in the skewness. We also study the 2-point cross-correlation of mass and halos which gives an idea of how important the stochasticity is in the bias relation.

The relation between the mass function and the bias can be inverted. Consequently one may use the bias as a proxy for the mass of the halo sample. This is of direct relevance to the interpretation of observational data. Systematic errors in estimating the mass from the bias would propagate to, and broaden, the constraints on cosmological parameters (like the dark energy equation of state parameter w) when fitted to the estimated halo mass function. Notice that self calibration methods for the mass function, which are expected to be used by DES-like surveys, assume that we know the mass-bias relation (Lima & Hu 2005, 2007). In this work we will assess how well the halo mass is recovered by using as input the clustering bias parameters from the two and from the 3-point correlation functions.

Going one step further, to relate halos to galaxies, it has become customary to use the Halo Occupation Distribution (HOD) prescription, which consists of populating either theoretically, or in the simulation, the dark matter halos with galaxies, using some simple (author-variable) population function that usually depends only on three or four parameters. The HOD prescriptions are far from providing a few percent precision of all measurements. For instance, Scoccimarro et al. (2001) found that they were unable to match both the variance and the skewness of APM galaxies. Since a local model of biasing is assumed along with the

bias prediction from the mass function, it is unclear if this disagreement is due to the HOD choice or to the failure of either the local model or the bias predictions. It is therefore of direct observational interest to assess each step separately, which is what this paper starts doing.

Indications that more work is needed to construct reliable galaxy mocks has been given by Guo and Jing (2009). Using a semianalytical mock sample of galaxies constructed from an N-Body simulation, they compared the local bias parameters from clustering with the local bias predicted using the peak background split Ansatz plus an HOD, which were found to be significantly different. Such difference may arise from the fact that the authors were using a published prescription instead of fitting their own HOD function, but part of the disagreement could come as well from the local bias and the PBS Ansatz.

Finally, note that we only study clustering in configuration space. Bias will most likely have different effects in Fourier space, in particular regarding shot-noise effects and stochasticity (see eg. Tinker et al. 2010, Seljak, Hamaus & Desjacques 2009, Cai, Bernstein & Sheth 2010, and references therein).

The paper is organized as follows. Section II gives a brief introduction to the simulations. In section III we study the performance of the local bias model in simulations and present a study of shot-noise and next to leading order contributions. In section IV we compare the clustering of halos in the simulations with the peak backgrounds split predictions and check how well we can recover the mass of halos from the bias parameters. We present our conclusions in section V.

2 NUMERICAL SIMULATIONS

In this paper we work with the comoving data from the MICE intermediate dark matter simulation, which has a volume of $V = (1536 Mpc/h)^3$ and $N = 1024^3$ particles, and consequently a mass resolution of $2.34\ 10^{11} M_\odot/h$ This simulation have been run with Marenostrum at the Barcelona Supercomputer Center using the L-GADGET code, periodic boundary conditions, and 128 processors. In this paper we use the $z = 0.0$ and the $z = 0.5$ comoving outputs. The cosmological model parameters for the simulation are $\Omega_m = 0.25$, $\Omega_\Lambda = 0.75$, $\Omega_B = 0.044$, $n_s = 0.95$, $h = 0.7$ and $\sigma_8 = 0.8$. The softening length of the simulation is 50 Kpc/h. The initial conditions were set at $z = 50$ using Zeldovich approximation. Halos have been found using a Friends of Friends algorithm with a linking length 0.168 times the mean interparticle distance, which results in 2729833 halos of more than 20 particles at z=0, and 2110669 halos at z=0.5. The effect of chancing linking length have been studied in Manera, Sheth and Scoccimarro 2010. By working with comoving data we concentrate on the gravitational evolution and structure formation and get rid of redshift distortions and other lightcone effects, which might not be directly related to the questions addressed here. Nevertheless, since at the end we want to model observational data, the inclusion of lightcone effects and redshifts distortions have to be considered as the natural next step in this study (see also Marin et al 2008).

3 LOCAL BIAS PERFORMANCE

A simple model for halo or galaxy bias was introduced by Fry and Gaztañaga (1993). These authors assumed that the density contrast in the halo (or more generally in the galaxy) distribution δ_h can be expressed as a non-linear function of the local density contrast of dark matter, δ_m, so that $\delta_h = F[\delta_m]$. On large enough smoothing scales, where the fluctuations are small, this relation can be expanded in a Taylor series

$$\delta_h = F[\delta_m] = \sum_{k=0}^{\infty} \frac{b_k}{k!}\delta_m^k = b_0 + b_1\delta_m + \frac{b_2}{2}\delta_m^2 + \cdots \qquad (1)$$

where $\delta_m(r)$ is the local density contrast at position r smoothed over a given characteristic R_s scale. With this local bias model, one can compute the 2 and 3-point halo biased correlation functions, to find (Fry & Gaztanaga 1993; Frieman & Gaztanaga 1994)

$$\begin{aligned} \xi^h(r_{12}) &\equiv < \delta_h(r_1)\delta_h(r_2) > \simeq b_1^2\ \xi(r_{12}) \\ Q_3^h(r_{12}, r_{23}, r_{13}) &\simeq \frac{1}{b_1}\ [Q_3(r_{12}, r_{23}, r_{31}) + c_2] \end{aligned} \qquad (2)$$

where $c_2 \equiv b_2/b_1$ and $\xi(r_{12}) \equiv < \delta_m(r_1)\delta_m(r_2) >$ is the 2-point matter correlation function. The distance r_{12} corresponds to the separation of two arbitrary positions 1 and 2. The hierarchical 3-point function, Q_3 has 3 such distances and is defined as

$$Q_3(\alpha) \equiv \frac{< \delta(r_1)\delta(r_2)\delta(r_3) >}{[\ \xi(r_{12})\xi(r_{23}) + \xi(r_{12})\xi(r_{13}) + \xi(r_{13})\xi(r_{23})\ ]} \qquad (3)$$

We need three parameters to specify the triangle formed by the 3 positions r_1, r_2 and r_3. We will fix two of these sizes (r_{12} and r_{13}) and show the results as a function of α, the angle between r_{12} and r_{13}. In general $Q_3(\alpha)$ has a characteristic U or V-shape (see Fig.6): is larger for small and large angles than for intermediate values.

There is ambiguity over what we should use as smoothing scale R_s in Eq. 1. A common and natural choice is that R_s should be smaller than r_{12}. But we will show that this does not provide a good model for $r_{12} < 60$ Mpc/h. Another possibility, that we will support here, is to think of an effective R_s that can be larger than r_{12}. Correlations are estimated from spatial averages over very large volumes and one can then think of Eq.1 as some average transformation over the whole volume. In this sense this bias transformation just provides an effective description which is only local over a very large smoothing radius.

When the correlation distances are zero we recover the corresponding relations between smoothed variances and skewness (see Eq.8).

$$\sigma_h^2 \simeq b_1^2\sigma^2 \ \ ; \ \ S_3^h \simeq (S_3 + 3c_2)/b_1 \qquad (4)$$

Here it is common to identify R_s with the smoothing scale in variance and skewness, but this does not need to be the case.

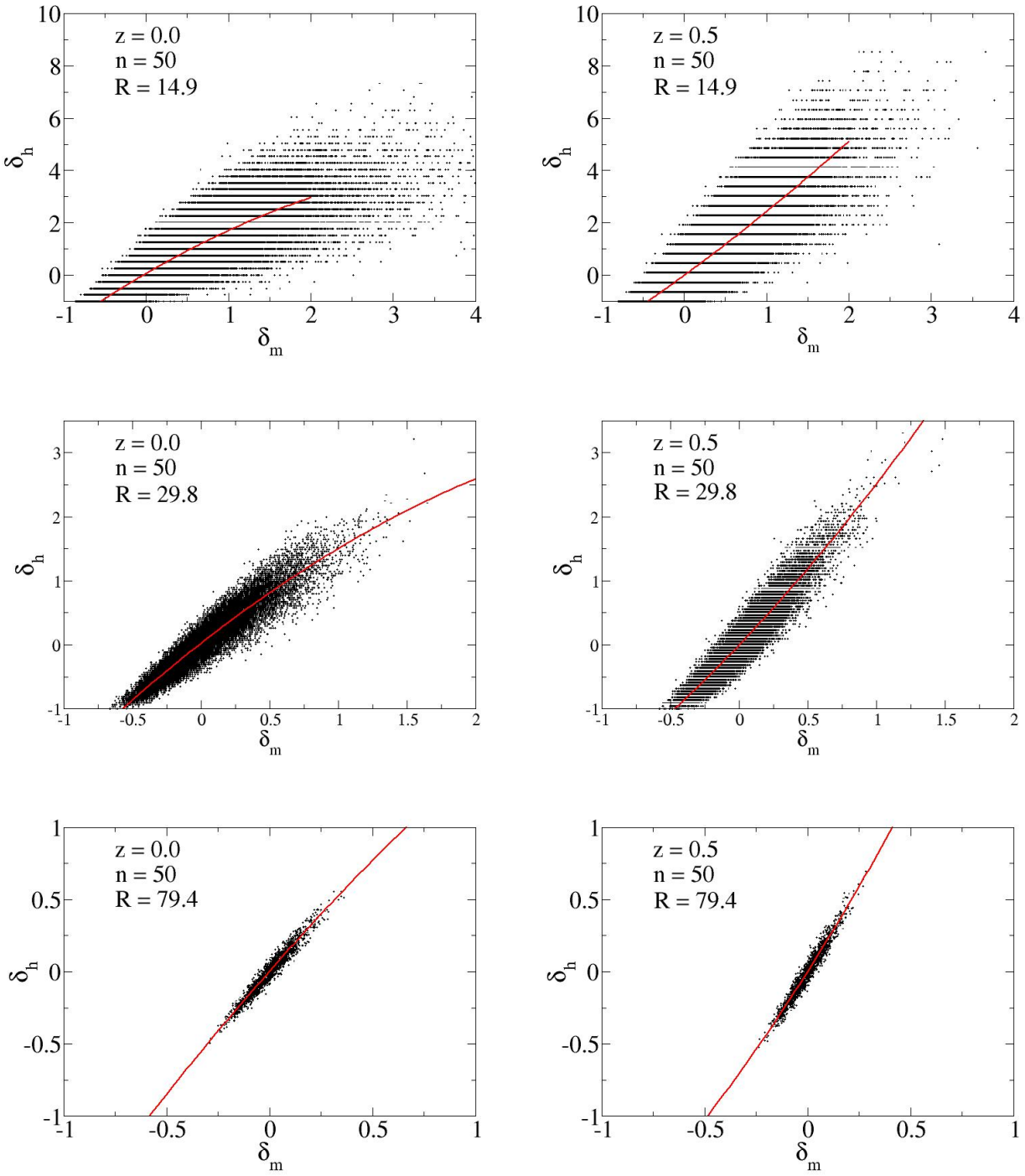

Figure 1. Scatter plots showing halo density contrast δ_h, smoothed over top-hat cells, for halos of 50 or more particles versus dark matter density fluctuations δ_m smoothed over the same cells. Results are shown for a different cell sizes with equivalent radius R_s as labeled in the figure. Results are for simulation data at redshift z=0 (left panels) and z=0.5 (right panels). In a continuous line we show the least square fit to the local bias parabola.

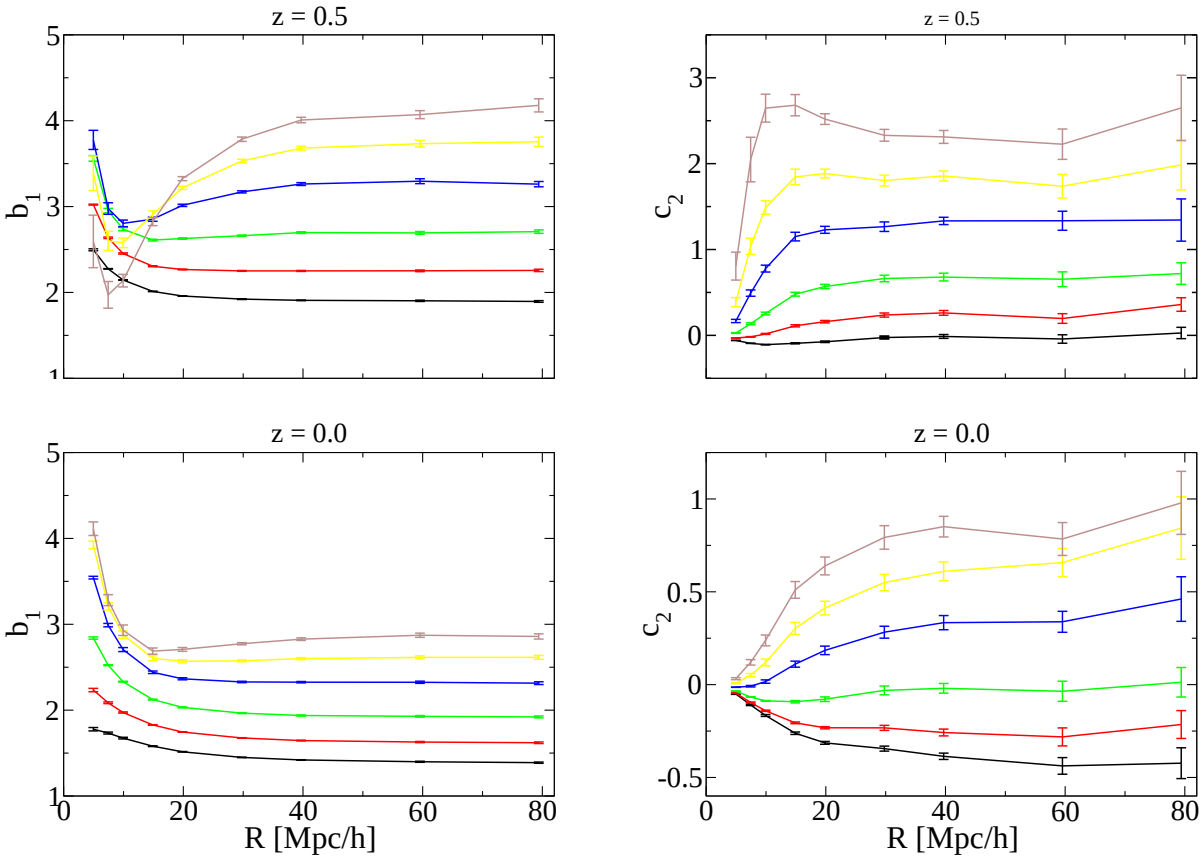

Figure 2. Variation of b_1 (left panels) and c_2 (right panels) as a function of the smoothing radius R. Top panels corresponds to $z = 0.5$ and bottom panels to $z = 0$. Results are shown for different minimum number of particles per halo, n. In each panel from bottom to top n=25 (black), n=50 (red), n=100 (green), n=200 (blue) and n=400 (yellow). Being the particle mass $23.42 \times 10^{10} M_\odot$ it yields, after correcting for resolution effects, minimum masses of 0.5 (black), 1.06 (red), 2.19 (green), 4.49 (blue), and 9.11 (yellow) $10^{12} M_\odot$

In the above equations, and also in Eq.2, the $\simeq$ sign indicates that this is the leading order in ξ. Note that in general, even when $\delta_m \ll 1$, the linear bias prescription (i.e., using only b_1) is not accurate for higher-order moments like Q_3, the reason being that nonlinearities in bias (i.e. c_2) generate non-Gaussianities of the same order as those of gravitational origin. In general, to predict higher order correlations in halo (or galaxies) to order N the local relation has to be expanded to order $N-1$ (Fry & Gaztanaga 1993). In this paper we will only study the clustering to order $N = 3$ which means that bias only needs to be quadratic in the local model. Thus, in practice, we will be testing the following model:

$$\begin{aligned} \delta_h &= b_0 + b_1\delta_m + \frac{b_2}{2}\delta_m^2 + \epsilon \\ &= b_1\delta_m + \frac{b_2}{2}(\delta_m^2 - \sigma_m^2) + \delta_\epsilon \end{aligned} \quad (5)$$

where ϵ represents the scatter around the local relation (and also includes higher order contributions in δ_m). Because we require $< \delta_h >= 0$, we have $b_0 = -b_2\sigma_m^2 - < \epsilon >$ and define $\delta_\epsilon \equiv \epsilon - < \epsilon >$.

One important prediction of this local model is to expect the shape of the correlation to be unaffected by bias (or in other words that the effective bias is constant) on large scales:

$$\xi^h(r_{12}) \simeq b_1^2\ \xi(r_{12}) + \mathcal{O}[\xi^2(r_{12})] \quad (6)$$

The next to leading contribution to ξ^h above is proportional to ξ^2 and consequently negligible at large r_{12} where $\xi < 1$. This will be tested below in section §3.3.

It is in principle possible to use the shape of Q_3^h in simulations (or observations) to separate b_1 from $c_2 \equiv b_2/b_1$. This is done by a fit of the halo (or galaxy) measurements of $Q_3^h(\alpha)$ in Eq.2 using the corresponding dark matter predictions or measurements $Q_3(\alpha)$. Changing b_1 will produce a distortion of the U-shape of Q_3 (as a function of α), while c_2 only produces a constant shift. Thus, unless Q_3 is constant within the errors or b_1 is very large, one could simultaneously measure b_1 and c_2 from Q_3^h (Frieman & Gaztanaga 1994; Fry 1994). This idea will be tested below in section §3.4. One could also predict b_1 from the ratio of the halo to dark matter correlations: $b_1^2 = \xi_h/\xi_m$, but this requires knowledge of the normalization of the dark matter clustering amplitude in ξ_m, which is often what we want to fit from observations. The fit to Q_3 can produce an estimate of the linear bias b_1 which is independent of the overall amplitude

of clustering ξ_m, because the Q_3 prediction is independent of the normalization. This approach has already been implemented for the skewness S_3 (Gaztañaga 1994, Gaztañaga & Frieman 1994), the bispectrum (Frieman & Gaztañaga 1994, Fry 1994, Feldman et al. 2001, Verde et al. 2002) or the angular 3-point function (Fry 1994, Frieman & Gaztañaga 1999, Gaztañaga & Scoccimarro 2005, Gaztañaga et al. 2005).

3.1 Measurements in δ_h vs δ_m scatter plot

We are interested in exploring and determining the local bias parameters directly. In order to do so we will compare the halo density contrast δ_h with the corresponding local matter density fluctuation δ_m at the same cells. We will do this for all cells in the simulation. This will give us an scatter plot of the relation $\delta_h = F[\delta_m]$ from which we can obtain b_1 and c_2 by means of a least mean square fit to the local bias parabola from the Taylor expansion of δ_h in Eq.5.

Scatter plots of halos of more than n=50 particles are shown in Fig.1 for a selection of sizes of the cubical cell ($l_c = 24, 48, 128$ Mpc/h), which correspond to spherical top hat volumes of radius $R_s = 14.9, 29.8, 79.4$ Mpc/h as labeled in the figures. Left and right panels show results for $z = 0$ and $z = 0.5$ respectively. It is apparent how the quadratic bias c_2 changes sign from convex ($c_2 < 0$) to concave ($c_2 > 0$) as the redshift increases.

One prominent feature in the plots is the discreteness of the δ_h values, i.e., that we see horizontal lines in the figures. This obviously comes from the fact that we have an integer number of halos in each cell. The step in the halo density fluctuations is consequently $\Delta\delta_h = 1/\bar{n}$, where $\bar{n}$ is the mean number of halos in the cells. This is the value of the Poisson shot-noise, which will decrease when increasing the cell size or when lowering the mass threshold of halos, for we will have a larger $\bar{n}$. The matter density field is also discrete, but because the large number of matter particles per cell this effect is not visible in the plots.

3.2 Smoothing scale

The bias parameters obtained from the least mean square fit depend on the size of the cell used to smooth the density field, therefore the issue of what smoothing radius to use when comparing with clustering bias should be addressed. First, notice that for the smallest smoothing radius the scatter of points is very big. In this case many points have $\delta_m \geq 1$, which situate us in a regime where the Taylor expansion of $F[\delta_m]$ can not be applied. When the radius is set to a larger value the scatter gets reduced and almost all points have $\delta_m < 1$, situating us within the perturbation regime and producing a particular fit of the bias parameters.

Our results of the dependence of the bias on the smoothing radius for several halo minimum masses are presented in Fig.2.

As expected, we see that the values of b_1 and c_2 change significantly as we increase the smoothing radius R_s from 5 to $20-25$ Mpc/h, from where they start to converge to their large scale values. The convergence is reached faster at lower mass thresholds and, for a fixed mass, at lower redshifts. In our study we will take smoothing radius of 30 and 60 Mpc/h, where the convergence regime has been reached.

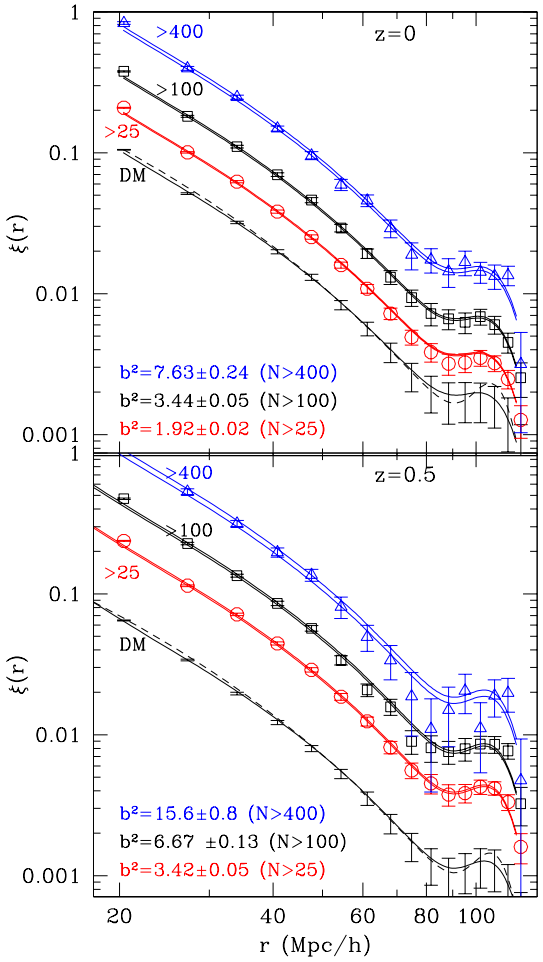

Figure 3. Symbols with JK errorbar show the 2-point correlation function $\xi(r)$ from simulations for different minimum number of particles ($N > 25, 100$ or 400) per halo as labeled in the figure. The bottom errorbars corresponds to the measurements in the DM distribution. The bottom continuous (dashed) lines in each panel shows the RPT (linear) theory prediction. The upper continuous lines show the best fit amplitude for the RPT prediction shape, whose amplitudes b^2 are shown in the bottom labels. Top (bottom) panel correspond to z=0 (z=0.5).

Through all the paper errors on the measured bias parameters have been computed using the jack-knife method with 64 subsamples of the density fluctuations field. This is, we first compute the density fluctuations using the true mean density of the simulation and then we create the jack-knife subsamples from which we obtain, using these fluctuations, a set of 64 bias. Applying equation 26 gives the estimated jack-knife error. We have check that changing the number of regions does not change results significantly.

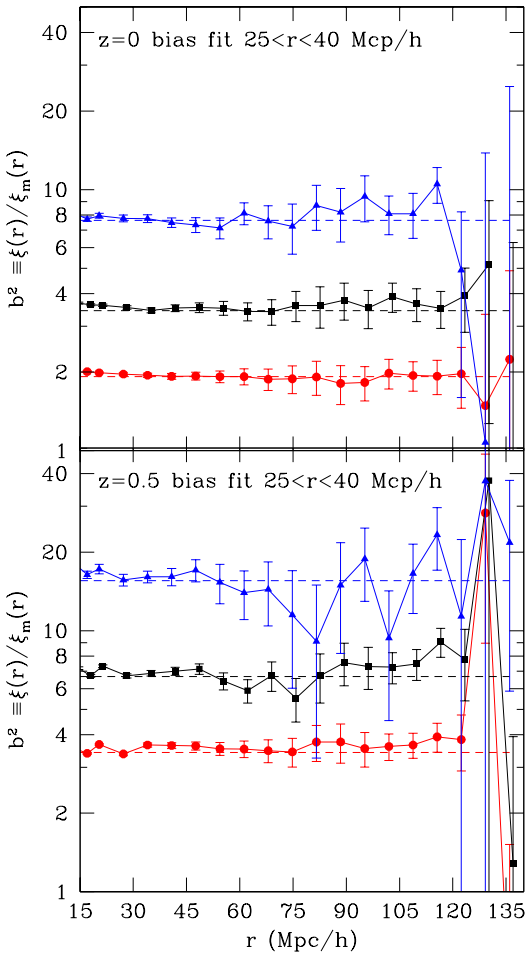

Figure 4. Bias from the ratio of 2-point correlation function $\xi(r)$ for different minimum number of particles per halo N=25, 100, 400 (from bottom to top). Top panel shows results for $z = 0$ and bottom panel for $z = 0.5$. The dashed lines show the values of the linear bias fit in the range $25 < r < 40$Mpc/h.

3.3 Comparison with 2-point correlations

We have computed the 2-point correlation function $\xi(r)$ for the matter and halo density contrast in the simulation. To estimate $\xi(r)$ we have used the 4Mpc/h density mesh of the simulation and average all the mesh points separated by $(r \pm \Delta r)$, where $\Delta r = 0.5 Mpc/h$ (see Barriga & Gaztanaga 2002 for details). The results for the matter correlation function and for different halo masses (given by the minimum number of particles per halo) are shown in Fig.3. The top panel shows the $z = 0$ case and the bottom panel the $z = 0.5$. To convert particles to halo mass remember that $M_p = 2.34\ 10^{11} M_\odot/h$.

As expected the more massive the halos the more biased the correlation function. Note as well what is called the stable clustering, i.e., the fact that for a given halo mass threshold the absolute value of ξ remains approximately constant in redshift while the matter correlation function decreases (in redshift). This could be understood however because halos of a given mass but at different redshift do not correspond to the same Lagrangian mass. The ones at higher redshift are situated in a rarer (less expected) matter fluctuations, being therefore more biased.

The measured correlation function from the simulation shows very clearly the acoustic peak at about $\sim 110 Mpc/h$ for both the matter and the halo functions. For comparison, in this figure we have also plotted the Linear Perturbation Theory (PT) prediction (dashed lines) and the Renormalized Perturbation Theory (RPT) prediction (continuous) for the correlation function, which has been kindly provided by M. Crocce The RPT shows deviations of the linear theory at much larger scales that have been previously thought and even in the acoustic peak scale one gets a contribution of the nonlinear effects (Crocce & Scoccimarro 2008). As can be seen in the figure these nonlinear contributions results into a smoother prediction for the acoustic peak shape in the RPT that is in better agreement with what we find in the simulations.

We find the bias from

$$b(r) = \sqrt{\frac{\xi^h(r)}{\xi^m(r)}} \qquad (7)$$

This bias is expected to be constant at large scales in the local bias model of Eq.6. Cosmic variance and shot-noise will add variations to this large scale constant bias. Both errors get more pronounced for larger scales (where we have few modes in the simulation) and for larger halo mass thresholds (since the number of halos is smaller). This can be seen in Fig.4 where we plot b^2 as a function of separation for redshifts $z = 0$ and $z = 0.5$ and different mass thresholds. We do not find any evidence in the data for scale variations of b for $r > 20$ Mpc/h. This favors the local bias model, but note that this statement is only accurate within the $\simeq 10\%$ accuracy in our analysis.

We do a fit to a constant $b(r)$, weighted by the inverse variance, for different range of scales. The result is shown as continuous lines in Fig.3 and triangles in Fig.5. The bias from $\xi(r)$ is slightly larger when we fit to smaller scales of $20 - 40 Mpc/h$, but results are consistent within errors. We can see in this later figure that, within its errors, the bias from clustering is in good agreement with the local bias determined directly from the δ_h-δ_m relation at larger scales. The values in the figure correspond to cell size $R_s = 60$ Mpc/h where the bias in Fig.2 has reach its asymptotic value for all masses. The agreement is no so good for smaller smoothing scales. Even for cells as large as $R_s = 30$ Mpc/h we find some deviations in b for large masses. This clearly indicates that the local bias prescription in Eq.1 is to be understood as an effective relation smoothed over very large scales and it fails when we try to apply it as a truly local transformation (where $R_s < r_{12}$, with $R_s < 60$ Mpc/h). Also note that at these large smoothings the stochastic component δ_ϵ (see Eq 5) is small as illustrated in Fig. 1 and that, in particular we can neglect the stochasticity correlation between two different points $< \delta_\epsilon(r_1)\delta_\epsilon(r_2) >$ in the modeling of the 2-point correlation.

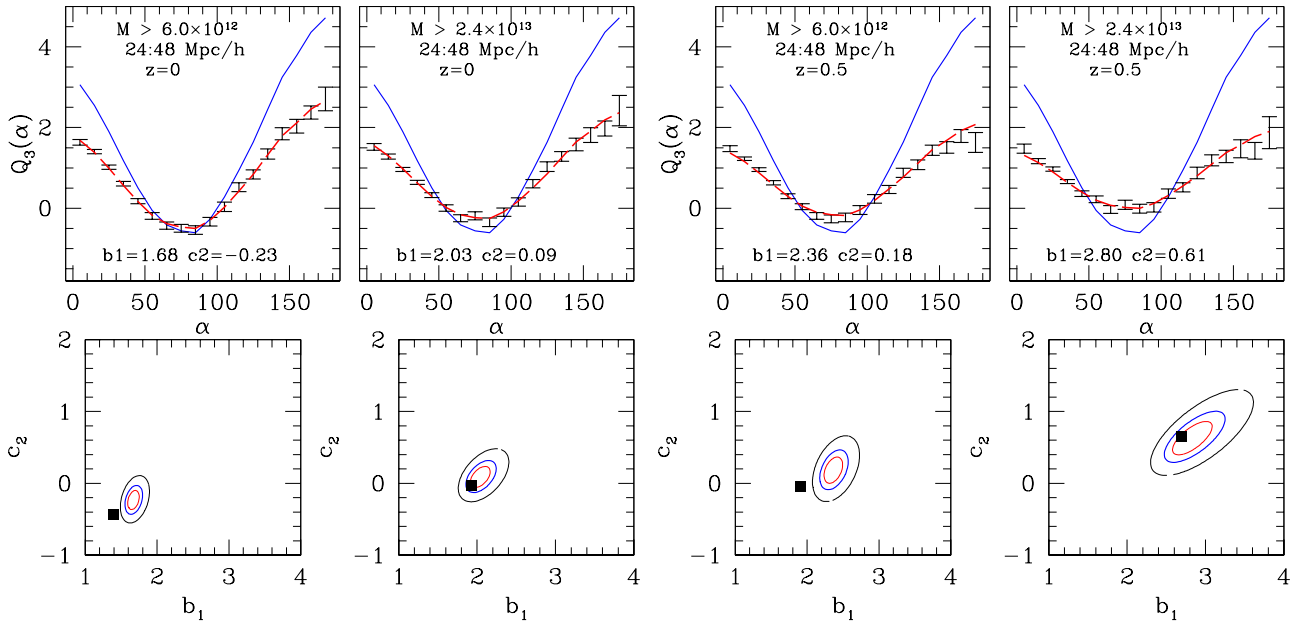

Figure 6. Halo biases from the reduced 3-pt function $Q_3(r_{23}, r_{12}, \alpha)$ for z=0 (left set of panels) and z=0.5 (right set of panels) with $r_{23} = 2r_{12} = 48$ Mpc/h. Each column corresponds to a different halo mass (as labeled in the top panels). **TOP**: Q_3^m in dark matter as measured in the simulation (blue lines) as compared to Q_3^h in halos (errorbars) of the same simulation. Long dashed red lines show the local bias model predictions (equation 2) for the best fit values of b_1 and c_2 shown in the bottom panels. **BOTTOM**: χ^2 contours in the $b_1 - c_2$ plane for $\Delta\chi^2 = 1, 2.3$ and 6.17. Best fit values are found by matching the measured Q_3^h in halos (symbols in top panels) with predictions in the local bias model, ie $Q_3^h = (Q_3^m + c_2)/b_1$ where Q_3^m are the dark matter values (blue continuous lines in top panels). Filled squares show the values of $b_1 - c_2$ from the local bias scatter plot $\delta_h - \delta_m$ in Fig.2 at R=60 Mpc/h.

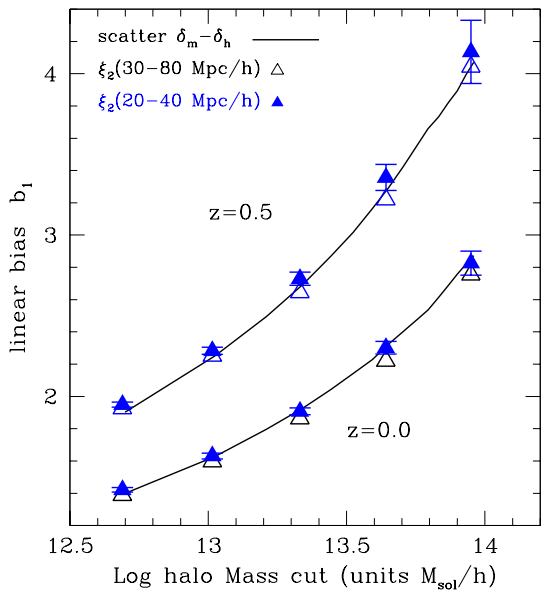

Figure 5. Comparison of different estimates for the linear bias as a function of the minimal halo mass. Continuous line correspond to the local model fit to the scatter relation $\delta_m - \delta_h$ in Fig.2 at R=60Mpc/h. Triangles correspond to bias from the 2-point function on large 30-80 Mpc/h scales (open triangles) and intermediate 20-40 Mpc/h scales (filled triangles).

3.4 Comparison with 3-point correlations

We have computed the hierarchical relation $Q_3(\alpha)$ (see equation 2) for dark matter and halos in the simulation (as for 2-point function we follow Barriga & Gaztanaga 2002). We use triangles with fixed $r_{23} = 2r_{12} = 48 Mpc/h$ and r_{13} given by the angle α between r_{23} and r_{12}. Some results for $z = 0$ (left) and $z = 0.5$ (right) are shown in Fig.6. Dark matter measurements are shown as (blue) continuous lines while halo measurements correspond to errorbars. Errorbars in dark matter are negligible as compare to errors in the halo distribution, which is dominated by shot-noise. The standard perturbation theory prediction for Q_3 is quite close to the DM measurements on these large scales. Notice the characteristic U shape in $Q_3(\alpha)$. This is an indication of filamentary structure, i.e, aligned structures ($\alpha \sim 0$, $\alpha \sim 180$ deg) are more probable than perpendicular configurations (for instance, equilateral triangles). Spherical structures will produce constant values of $Q_3(\alpha)$. As the bias increases, the distribution becomes less filamentary and this information can be used to measure the bias.

We have fitted the shape of Q_3^h in simulations to b_1 and c_2 in Eq.2 using the corresponding dark matter measurements Q_3 (we follow the procedure described in Gaztañaga & Scoccimarro 2005) Changing b_1 produces a distortion of the U-shape of Q_3, while c_2 only produces a constant shift. The fits are shown as contours in the bottom panel of Fig.6 and they are compare with the values of b_1 and c_2 (squares) from the scatter plot in Fig.2 at $R_s = 60$ Mpc/h. For er-

rorbars we use the JK covariance matrix. This matrix is degenerate because of the strong correlations of different α bins. To be safe we only use the two principal components with larger eigenvalues (see Gaztañaga & Scoccimarro 2005). This is quite conservative in terms of the size of the resulting errorbars. Better estimates would require a more careful study of the covariance matrix, which is beyond the scope of this paper.

The values of b_1 recovered from Q_3 (squares) for different mass thresholds are shown in Fig.7. There is good agreement in the general tendency of b as a function of mass but there are some significant deviations for small masses ($\log M < 13$). This failure of the local biasing model for Q_3 is intriguing in the light of the very good agreement that we found from ξ in Fig.5. This is an important point to clarify because we do not know b_1 in the real universe and we were hoping to be able to use the values of b_1 from Q_3 to find the dark matter normalization of ξ. According to Fig.7 this will produce a significant (2-sigma level) deviation for small halo masses.

This mismatch can hardly be attributed to the stochastic component δ_ϵ (which includes also non-local contributions). As in the case of the 2-point function, because the smoothing radius in the local model is very large, we expect the stochastic correlation components to be subdominant (see section above). A key difference between the 2 and the 3-point function is that the former takes isotropic averages while the later keeps anisotropic information (something which is not captured either by the skewness, see below, which is a third order statistics but is smoothed in spherical cells). So our finding hint in the direction that we need some anisotropic component to the halo biasing model in Eq.1, at least for $\log M \simeq 13$. This conclusion might not be generic. For biasing in galaxy mock catalogs where $b \simeq 1$, corresponding to lower mass thresholds in the halo picture, Gaztañaga & Scoccimarro (2005) and Marin et al. (2008) found good agreement of the values of b_1 coming from ξ and Q_3 clustering under the local model. More work needs to be done to clarify these issues.

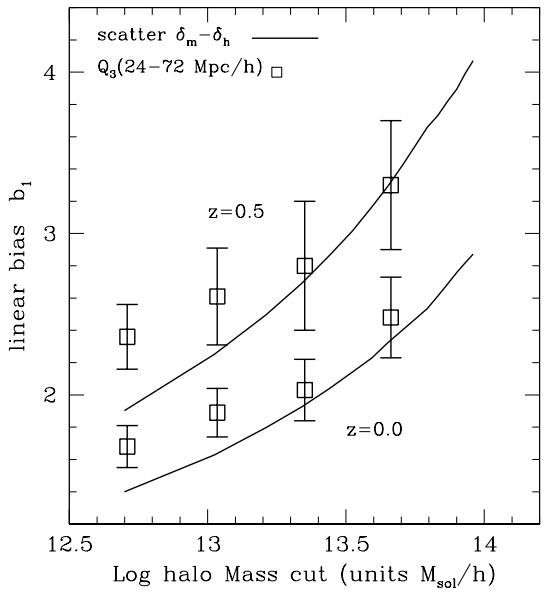

Figure 7. Comparison of different estimates for the linear bias as a function of the minimal halo mass. Continuous line correspond to the local model fit to the scatter relation $\delta_m - \delta_h$ in Fig.2 at $R_s = 60$Mpc/h. Open squares come from fitting the 3-pt function Q_3, i.e., see Fig.6.

3.5 Comparison with the variance and skewness

So far we have studied the bias from 2-pt and 3-pt correlation functions because they do not suffer from the discreteness effects that appear in the variance and the skewness. However, the latter are closer to the local model assumptions (since they prove a local smoothed quantities). Since they bring different aspects to the comparison we will also study them here.

We define the variance σ^2 and skewness m^3 as second and third order moments of the fluctuation field:

$$\sigma^2 = \langle \delta^2 \rangle = \frac{1}{N}\sum_{i=1}^{N} \delta_i^2 \ ; \ m_3 = \langle \delta^3 \rangle = \frac{1}{N}\sum_{i=1}^{N} \delta_i^3 \qquad (8)$$

where the sum is over a fair sample of points in the simulation (ergodic assumption). In this case, one typically considers these quantities as a function of the smoothing radius R. It is also convenient to define the normalized skewness:

$$S_3 = \frac{m_3}{\sigma^4} \qquad (9)$$

3.5.1 Variance

One of the common ways of determining the linear bias of galaxies or halos is by comparing their variance with the measured/predicted matter variance. However, to do the correct comparison one has to account for the shot-noise contribution (a very similar problem occurs in the estimation of the power spectrum which is the variance in Fourier space). This contribution to the variance appears because galaxies and halos are not a continuous fields, but discrete ones. For a top hat window function, $W_R(r) = \Theta(\mid r \mid - R)$ the Poisson shot-noise is well known and it is equal to $1/\bar{n}$ where $\bar{n}$ is the mean number of halos in a sphere of radius R. The shot-noise corrected variance is therefore:

$$\sigma^2(R) = < \delta^2 > - \frac{1}{\bar{n}} \qquad (10)$$

where R stands for the window function smoothing scale. The dark matter in the simulation is also a discrete field and, as mentioned before, it will have its own shot-noise correction, which will obviously be much smaller than the halo one due to its higher number density. Now, we can use the halo variance to compute an estimator for the linear bias as

$$b_{hh} \equiv \frac{\sigma(R)}{\sigma_m(R)} = \sqrt{\frac{< \delta_h \delta_h > -1/\bar{n}}{< \delta_m \delta_m >}} \qquad (11)$$

Another estimator for the linear bias that can be computed from the simulation is

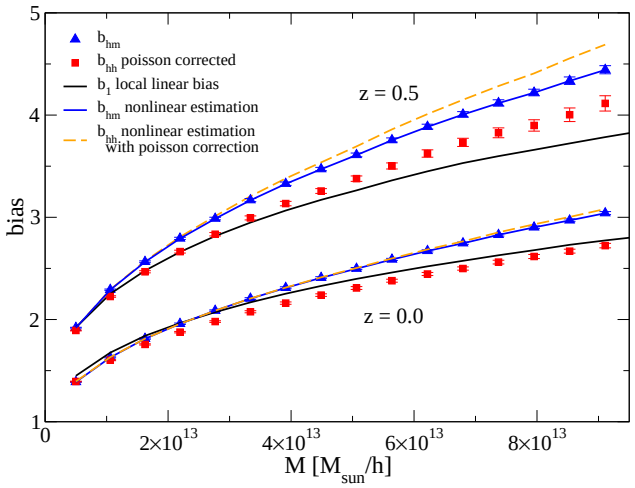

Figure 8. Bias as a function of halo mass. The linear bias b_1 (shown as black lines) is estimated from a fit to the scatter plot δ_h-δ_m in the simulations. This is compared with the bias values obtained from the (shot-noise corrected) variance $b_{hh} = \sigma/\sigma_m$ (red squares) and from the cross-correlation $b_{hm} =< \delta_m\delta_h > /\sigma_m^2$ (blue triangles). Also shown are the predictions for b_{hh} and b_{hm} after applying non-linear contributions (i.e., in Eq.16 and Eq.17). Results are shown for both $z = 0$ (bottom lines and symbols) and $z = 0.5$ (on top).

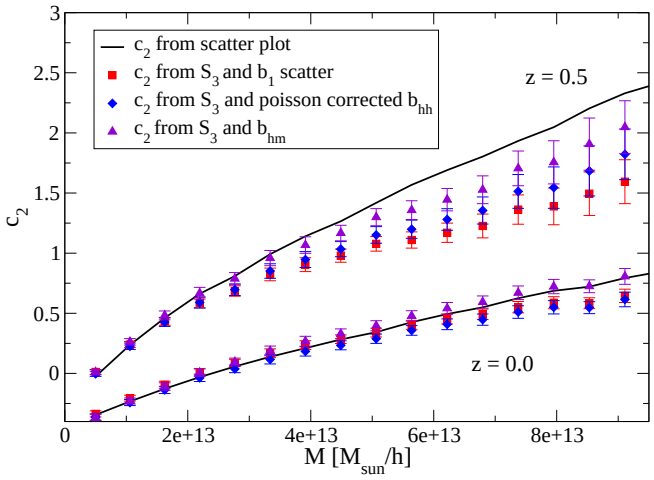

Figure 9. Dependence of c_2 on the halos mass as measured directly from the δ_h-δ_m local relation in the simulation (black lines) compared with the values obtained from the skewness and three different linear bias estimates in Eq.15: b_1 from the local relation (red squares), b_{hh} (blue diamonds) and b_{hm} (pink triangles). Top (bottom) set of lines are for $z = 0$ ($z = 0.5$).

$$b_{hm} \equiv \frac{< \delta_h\delta_m >}{< \delta_m\delta_m >} \tag{12}$$

In Fig.8 we show the values for the different bias estimators computed in cubical cells of side $l_c = 48$ Mpc/h. The variance in a cubical cells is very similar to the one in a top hat smoothing sphere of equal volume as the cube (Baugh, Gaztanaga & Efstathiou 1995). For our cells of side $l_c = 48$ Mpc/h the spherical equivalent radius is $R = 29.8 Mpc/h$. Errors in the figure are from the Jack-knife method with 64 regions, and we have checked that changing the number of regions does not change results significantly.

We can see that all three bias estimators b_1, b_{hh} and b_{hm} give significant different results given the errorbars. Consequently one needs to be cautious when trying to use these bias estimators for precision cosmology where errors lower than 10% are sought. Below we discuss the origin of these differences focusing mainly in non-linear and discreteness effects, which we find are the dominant effects. Other contribution could arise from the truncation of the Taylor expansion.

3.5.2 Skewness

An important clustering statistic for understanding quadratic bias is the skewness. As all the moments and cumulants of the halo field it has to be shot-noise corrected. For the normalized skewness this correction is found to be (eg. see Gaztanaga 1994):

$$S_3(R) = \frac{< \delta^3 > -3\sigma^2(R)/\bar{n} - 1/\bar{n}^2}{\sigma^2(R)} \tag{13}$$

where σ^2 is again the shot-noise corrected variance and R stands for the window function smoothing scale. Note that when comparing the measured skewness to predictions one has to take into account the fact that we are smoothing the density field. For a top hat smoothing and CDM power spectrum the normalized skewness can be approximated by (Juszkiewicz, Bouchet & Colombi 1993; Cooray & Sheth 2002; Bernardeau et al. 2002)

$$S_3 = 4 + \frac{6}{7}\Omega_m^{-2/63} + \gamma_1 \tag{14}$$

where $\gamma_1 = \frac{dln(\sigma^2(R))}{dln(R))}$. Obviously for the Einstein-de-Sitter cosmology and no smoothing we recover the well known value in the spherical collapse model 34/7 (see Fosalba & Gaztanaga 1998 for the interpretation in terms of the spherical collapse model).

With the skewness and the linear bias we can easily compute c_2 as (see section §2)

$$c_2 = (S_3^h\, b_1 - S_3^m)/3 \tag{15}$$

Here we can either use the direct local b_1 as measured from the $\delta_h - \delta_m$ scatter plot or other estimators of the linear bias as b_{hm} or b_{hh}. Results are shown in Fig.9 and compared with the c_2 obtained directly from the $\delta_m - \delta_h$ scatter plot fit. Errors for these points are computed by means of the Jack-knife method with 64 subsamples in the simulation. As in the case of the variance we find significant deviations between the different estimators. Next-to-leading order contributions as well as modeling stochasticity would be needed for precision cosmology.

3.6 Non-Linear effects and stochasticity

In order to asses how good the linear approximation is we compute the nonlinear contribution to the linear bias b_{hm} and b_{hh} using Eq.5. We start with b_{hm} which should be subject to smaller discreteness effects. The next order in σ^2 is:

$$b_{hm} = \frac{< \delta_m \delta_h >}{< \delta_m \delta_m >} = b_1 + \frac{1}{2} b_2 S_3 \sigma_m^2 + b_\epsilon \qquad (16)$$

where $b_\epsilon \equiv \frac{<\delta_m \delta_\epsilon>}{<\delta_m \delta_m>}$, and $\delta_\epsilon = \epsilon - < \epsilon >$. Because of symmetry reasons, b_ϵ can be expected to be very small, as we will show next.

Nonlinear corrections in Eq.16 seem to account well for the difference that we saw in Fig.8 between the measured b_{hm} (blue triangles) and the linear bias b_1 (black continuous line) from the fit to the scatter plots. The non-linear correction to b_{hm} in Eq.16 is also shown in Fig.8 as a blue line (for $b_\epsilon = 0$) and it overlaps well with the b_{hm} measurements within errors. The nonlinear terms are therefore large (10-15% effect) and certainly have to be taken into account in precision cosmology. We infer from this very good agreement that the contributions from the scatter b_ϵ in Eq.16 and the effect of the Taylor truncation (i.e., higher orders in the expansion) are negligible given the errors.

The corresponding corrections for b_{hh} is:

$$b_{hh}^2 = b_1^2 + \left[b_1 S_3 + \frac{1}{2} b_2 + \frac{1}{4} b_2 S_4 \sigma_m^2 \right] b_2 \sigma_m^2 + \mathcal{E}_{hh} \qquad (17)$$

where the second term includes all the non-linear corrections and the third term is:

$$\mathcal{E}_{hh} = b_1 b_\epsilon + \frac{< \delta_m^2 \delta_\epsilon >}{\sigma_m^2} + \frac{< \delta_\epsilon^2 > - 1/\bar{n}}{\sigma_m^2} \qquad (18)$$

which only includes terms involving the scatter. As pointed out above, because of symmetry, we expect linear terms in δ_ϵ to vanish so that $< \delta_\epsilon \delta_m^n > \simeq 0, n = 0, 1, 2$. This is well supported by the good agreement that we found above between b_{hm} in Eq.16 (with $b_\epsilon \simeq 0$) and measurements in Fig.8. But this might not be necessarily the case for the quadratic term $< \delta_\epsilon^2 >$ because there is no cancellation between positive and negative fluctuations. The $1/\bar{n}$ term comes from the shot-noise correction (i.e., Eq.11) which allows us to move from the discrete to the continuous halo variance; it assumes that halos are a Poisson sample of the dark matter field. If all scatter $< \delta_\epsilon^2 >$ in the local relation were just Poisson, then we expect that $\mathcal{E}_{hh} \simeq < \delta_\epsilon^2 > - 1/\bar{n} \simeq 0$.

In Fig. 8 we show how the non-linear corrections in Eq.17 fail to explain the difference between b_{hh} and b_1. The predicted b_{hh} (dashed line) is higher that b_{hm} (blue triangles) while the measured one (red squares) is lower. In fact, the nonlinear terms seem to increase the differences between the predicted and measured bias. This could be explained if $\mathcal{E}_{hh}$ turns out to be negative, which would happen if the scatter is sub-Poisson (smaller than Poisson) and consequently we overcorrected shot-noise it by using $1/\bar{n}$ term. Sub-Poisson shot-noise have been found in simulations (Casas-Miranda et al. 2002) for halos larger than $M_\star$.[2]

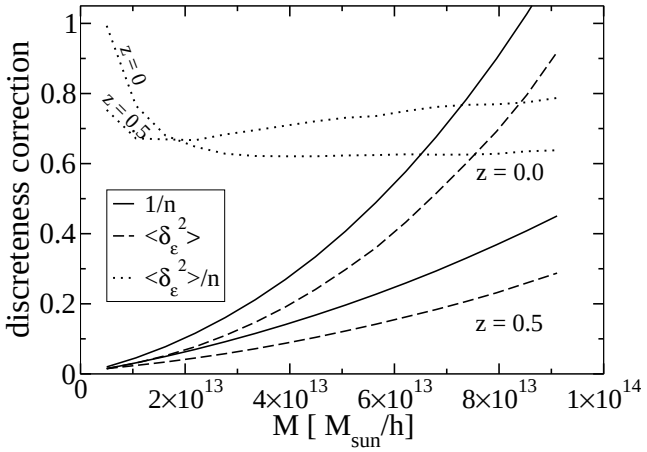

Figure 10. Comparison of the Poisson shot-noise correction $1/\bar{n}$ (continuous line) and the scatter $< \delta_\epsilon^2 >$ (dashed line) in the local bias. There are two sets of lines, one for each redshift as labeled in the figure (larger values correspond to $z = 0$). Dotted lines show σ_ϵ^2, the ratio of the two in Eq.19.

We have indeed found that our halo simulations have $< \delta_\epsilon^2 >$ which is smaller than $1/\bar{n}$. This can be seen in Fig.10, which compares the two terms. Besides shot-noise or discreteness effects $< \delta_\epsilon^2 >$ also include other sources of scatter: non-deterministic bias and possibly higher order contributions than the quadratic terms in Eq.5. The later is a smoothed component and is unlikely to result in a major increase in the actual scatter. Fig.10 therefore indicates that the final scatter is overestimated by the Poisson model. We can write the new effective shot-noise term as:

$$< \delta_\epsilon^2 > \equiv \frac{\sigma_\epsilon^2}{\bar{n}} \qquad (19)$$

where σ_ϵ^2 is plotted as dotted lines in Fig.10 . For small halo masses σ_ϵ^2 tends to unity, while it is roughly constant $\sigma_\epsilon^2 \simeq 0.6 - 0.8$ for larger masses.

In Fig.11 we apply the discreteness correction to the prediction rather than to the measurements (which are not corrected here for Poisson shot-noise). When we use the new estimate for the scatter, i.e., $\mathcal{E}_{hh} \simeq < \delta_\epsilon^2 >$ we find a very good match between the predictions and the measurements for b_{hh}, We can see here that, as happened for b_{hm} in Fig.8, non-linearities are also important for the variance. The main difference between b_{hm} and b_{hh} is that the later also needs a shot-noise correction that is different from Poisson, at least for large halo masses. Both discreteness and and non-linearities are needed to interpret the bias from the variance.

[2] Also note that the same effect seems to result in super-Poisson errorbars (Cabre & Gaztanaga 2009). This two statements are not in contradiction because the former refers to the Poisson correction to the mean variance (in Fourier or configuration space) while the later refers to the noise or error (around the mean 2-point function) induced by discreteness noise.

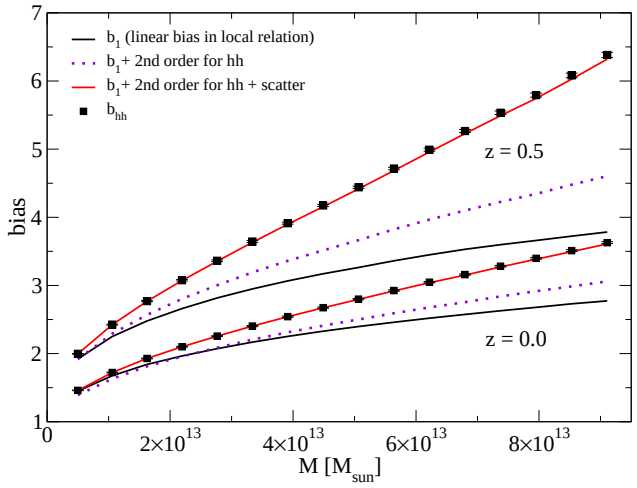

Figure 11. Bias in b_{hh} as a function of halo mass as in Fig.8 but here we do not apply the Poisson shot-noise correction to the measurements of b_{hh}. When apply instead the discreteness correction to the predictions (this correction estimated from the scatter $< \delta_\epsilon^2 >$ shown in Fig.10). We only find a good agreement between the non-linear predictions (red lines) and measurements (squares) after both discreteness and non-linear terms are included.

3.7 Cross correlation and stochasticity

A simple measure to study deviations away from the local linear bias relation has been pointed out by several authors (see Tegmark & Peebles 1998, Dekel & Lahav 1999, Seljak, Hamaus & Desjacques 2009, Cai, Bernstein & Sheth 2010, and references therein). This is to consider the dimensionless cross-correlation coefficient between the distribution of mass and galaxies (we use halos as a proxy for galaxies in our case):

$$r \equiv \frac{< \delta_m \delta_h >}{\sqrt{< \delta_m \delta_m >< \delta_h \delta_h >}} \qquad (20)$$

which is in general a function of scale. In the local linear bias model $r = 1$. But both non-linearities and stochasticity (the scatter around the local relation) can change this away from one. Note that this test is fundamentally different from previous test of the local bias. This test focus on how important is the stochasticity in the bias relation. For a deterministic function one expects $r = 1$, but when the scatter in the $\delta_h - \delta_m$ relation is large one would expect that it could have a different impact in both parts of this ratio.

For 1-point smoothed fields we have that in our notation (see Eq.11-12) this corresponds to:

$$r = \frac{b_{mh}}{b_{hh}} \qquad (21)$$

We can estimate this quantity directly from the variance measured in simulations. The result is shown in Fig. 12 as a function of halo mass. We compare measurements without any correction (lower lines) and using two different ways to correct for scatter and discreteness effects in the halo variance: the Poisson corrected variance: $< \delta_h^2 > -1/\bar{n}$ and the scatter corrected variance $< \delta_h^2 > - < \delta_\epsilon^2 >$. The cross-correlation deviates significantly from unity if we do not correct from these effects. Deviations increases with halo mass and redshift, and can be as large as 20-30% for large halos. As shown before (eg. see Fig.10) the Poisson model does not provide a good correction for the scatter. If we use instead the scatter away from the local relation, as measured in the simulation, we recover values which are close to unity.

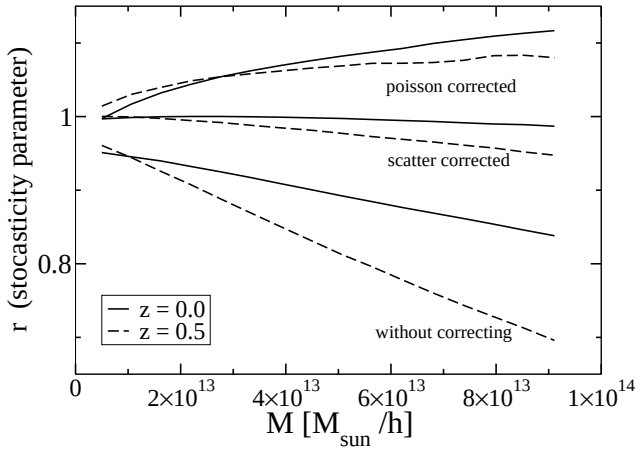

Figure 12. Dimensionless cross-correlation coefficient r in Eq.20 as a function of halo mass. This is for 1-point fluctuations smoothed over cells of $R \simeq 30 Mpc/h$ radius. Different pairs of lines show results using different ways to correct for the discreteness in the halo variance. Dashed (continuous) lines correspond to $z = 0.5$ ($z = 0.0$).

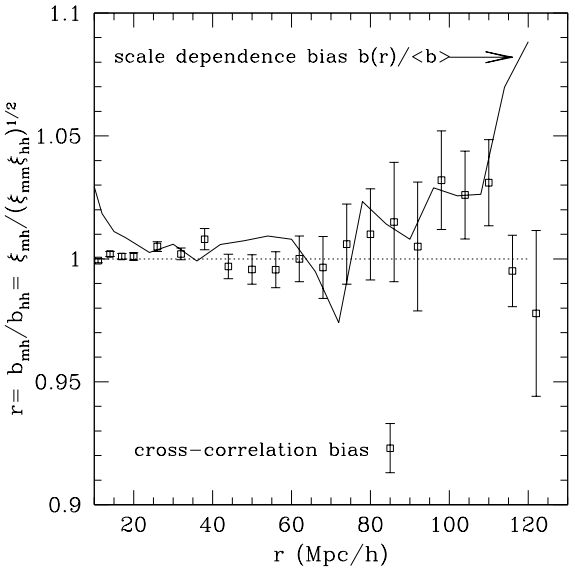

Figure 13. Symbols with errorbars show r in Eq.20, i.e., the dimensionless cross-correlation coefficient between dark matter and halos with $M > 5 \times 10^{12}$ in the MICE simulation at $z = 0.5$. The continuous line correspond to the scale dependence bias b_{hh}, normalized to the mean value.

We can also estimate r in the 2-point correlation function, which should be less affected by discreteness effects. Fig.13 shows r as a function of scale (separation between pairs) for halos with $M > 5 \times 10^{12} M_\odot$. In Fig.13 we estimate JK errors from the r ratio, i.e., we estimate the ratio in different JK subsamples and calculate the error from the scatter in the JK regions (this produces smaller errorbars because sampling variance mostly cancels in doing the ratio). For comparison we also show in this figure (continuous line) how much b_{hh} deviates from a constant (i.e., from Fig.4). The measurements are compatible with unity for all scales. There is a hint of a deviation ($\simeq 3\%$) around the BAO scale which could be related to recent findings about scale dependence bias (eg. see Desjacques et al. 2010 and references therein).

Similar results, but with much larger errors, are found for larger halos masses and different redshifts. Note that for masses larger than $10^{14} M_\odot$ Manera et al. 2010 found b_{hm}/b_{hh} to be slightly larger than unity, with b_{hm} measured at low k in Fourier space and b_{hh} at large separations in the autocorrelation function.

Altogether, our analysis indicates that the linear local bias model provides a very good approximation, within our sampling errors, for the 2-point function. On scales larger than $r \simeq 20 Mpc/h$, the halo-halo correlation and halo-mass correlations are, to a good approximation, linear tracers of the underlying dark-matter correlation function and the resulting bias is just the one expected in linear theory. This conclusion is important to interpret measurements of redshift space distortions and BAO in galaxy surveys, which on large scale usually are interpreted under the assumption that linear bias and linear theory are good approximations.

This is not so much the case for the variance, which seems more affected by non-linearities and discreetness effects. This is understood from the fact that the variance (as well as the power spectrum) is quadratic in fluctuations and is an average over all scales, including small, non-linear, scales.

4 BIAS PREDICTIONS FORM THE MASS FUNCTION AND THEIR PERFORMANCE

In the previous section we have studied how the local bias performs when compared with the bias measured from clustering. In this section we will compare those bias with predictions from the mass function.

4.1 Bias predictions from the mass function

In the peak-background split Ansatz (Bardeen et al. 1986; Cole & Kaiser 1989) one can relate the halo bias with the halo mass function at large scales by treating perturbed regions as if they were unperturbed regions in a slightly different background cosmology universe but one of the same age (Martino & Sheth 2009).

Consequently, from a well motivated functional form of the mass function, one can derive theoretical predictions for the halo bias parameters as well as study their accuracy (Mo et al. 1997, Scoccimarro et al. 2001, Cooray & Sheth 2002, Manera et al. 2010).

In this paper we will use the Sheth and Tormen (1999) mass function:

$$n(m)dm = \frac{\rho_m}{m} f(\nu) d\nu \quad (22)$$

$$\nu f(\nu) = A(p) \left(1 + (q\nu)^{-p}\right) \left(\frac{q\nu}{2\pi}\right)^{1/2} \exp\left(-\frac{q\nu}{2}\right). \quad (23)$$

where $A(p) = [1 + (2^{-p}\Gamma(1/2 - p))/\sqrt{\pi}]^{-1}$. is the normalized amplitude. The corresponding bias predictions are

$$\begin{aligned} b_1(m,z) &= 1 + \epsilon_1 + E_1 \\ b_2(m,z) &= 2(1+a_2)(\epsilon_1 + E_1) + \epsilon_2 + E_2 \end{aligned} \quad (24)$$

where $a_2 = -17/21$, and

$$\begin{aligned} \epsilon_1 &= \frac{q\nu - 1}{\delta_{sc}(z)} \qquad \epsilon_2 = \frac{q\nu}{\delta_{sc}(z)} \left(\frac{(q\nu)^2 - 6q\nu + 3}{\delta_{sc}(z)}\right) \\ E_1 &= \frac{2p/\delta_{sc}(z)}{1 + (q\nu)^p} \qquad \frac{E_2}{E_1} = \frac{1+2p}{\delta_{sc}(z)} + 2\epsilon_1 \end{aligned} \quad (25)$$

Throughout the paper $\nu = \delta_{sc}^2(z)/(D^2(z)\sigma_0^2(m))$. In this notation $D(z)$ is the growth factor in units of its value at $z = 0$; $\sigma_0(m)$ is the linear variance of the matter field at redshift $z = 0$, when smoothed with a top hat filter of radius $R = (3m\bar{\rho}/4\pi)^{-1/3}$ and $\delta_{sc}(z)$ is the critical density contrast for collapse at a given redshift z. Although it is popular in the literature to use a fixed value for δ_{sc} we will be using its proper redshift dependence from the spherical collapse (Eke et al. 1996, Cooray & Sheth 2002) since there is some indications that in this case the mass function closer to universal (Manera et al. 2010).

These predictions for the bias depend on the mass function through the parameters p and q. When $p = 0$ and $q = 1$ we recover the Press-Schechter (Press & Shechter 1974) formula. Original values for this mass function fit were $p \simeq 0.3$ and $q \simeq 0.7$ (Sheth & Tormen 1999) which discusses afterwards that $q = 0.75$ (and therefore $A \simeq 0.3222$) gives better results (Sheth & Tormen 2001; Cooray & Sheth 2002). We confirmed that this is the case and consequently we will use the latter values as their fiducial values for the ST. At the same time we will also use our own set of p and q values obtained by fitting the mass function as we explain in section 4.2. Bias parameters from a mass function with a functional form like that Warren et al. (2006) has been studied by Manera et al. (2010) and showed to give similar results than that of ST for a range of masses similar to that of this paper.

The above $b_i(m)$ predictions are for a given halo mass, but the simulation results are for halos above a mass threshold, consequently in this paper we integrated these predictions over the mass range, weighting appropriately according the number of halos at each mass. If one has a model for populating galaxies in halos one can weight each halo by the number of galaxies given by the halo occupation distribution (HOD), and therefore obtain a prediction for the galaxy bias. For an approach of how this can be done see for instance, Sefusatti & Scoccimarro (2005) or Tinker & Wetzel (2010). In this paper we are interested in separating these

two steps and understanding the errors that come from the halo predictions for clustering.

4.2 Mass function fits

We have computed the mass function of halos for the MICE simulation. We show it in Fig.14. Halos have been found using a Friends of Friends algorithm with a linking length 0.168 times the mean interparticle distance, and their masses have been corrected for discreteness effect following Warren et al. (2006), i.e., the mass of the halo have been set equal to $M_p\, N(1-N^{-0.6})$ where N is the number of particles and M_p the particle mass (which is $2.34\ 10^{11} M_\odot$ in our simulation). The Warren correction has been experimentally set using a linking length equal to 0.2 times while we are using 0.168. Differences in the correction, however, are very likely to be minimal if not negligible for the halo mass range in which we fit the mass function. Notice also that Crocce et al. (2009) has tested this correction for MICE simulations by means of randomly removing a fraction of the dark matter particles as a way of lowering the mass resolution, and found it to work quite well.

We have performed a χ^2 fit to the mass function data, starting from different lower mass thresholds for halos. Best fits for Sheth and Tormen (ST) functional form are shown as dashed colored lines in Fig. 14 (top panel), while data is in black dots. The fits are dominated by the lower mass bins which have smaller errorbars. For comparison we have added a line showing the mass function with the commonly used ST fiducial values $(p, q) = (0.3, 0.75)$. To appreciate better the differences between fits we show, in the bottom panel, the ratio of the best fit curves to that of the ST fiducial case.

The values for p and q of each fit and their statistical errors are shown in the Table 1. Errors come from jack-knife subsampling and are computed in the following way. We divide our simulation in 64 compact regions with equal volume. Then we create a set of $J = 64$ jack-knife subsamples of the data by removing each time one of these regions from the whole sample. For each jack-knife subsample we compute the mass function and fit its (p, q) parameters. Errors are then obtained as

$$(\Delta\theta)^2 = \frac{(J-1)}{J}\sum_{j=1}^{J}(\bar{\theta}-\theta_j)^2 \qquad (26)$$

where θ is a generic name of any of the parameters in which we are interested, in this case p and q, and $\bar{\theta}$ is the average of θ over the jack-knife subsamples. And for the best fit values of our parameters we take $\bar{\theta}$. When doing the χ^2 fit, errors in the mass functions are taken to be Poisson but results do not change significantly if they are estimated by the jack-knife method as well. Similar results are obtained if we divide the simulation in 27 jack-knife regions instead of 64. As it is shown in Table 1 we find that jack-knife errors on of p and q are smaller than the systematic errors that we are trying to asses by setting different halo mass thresholds.

$log(M_{min})$	z	p	q	σ_p	σ_q
13.0	0.0	0.334	0.665	0.001	0.003
13.5	0.0	0.309	0.733	0.002	0.004
14.0	0.0	0.275	0.786	0.004	0.006
13.0	0.5	0.347	0.691	0.001	0.003
13.5	0.5	0.312	0.763	0.003	0.004
14.0	0.5	0.280	0.801	0.010	0.011

Table 1 Best fit values of the Sheth and Tormen's p and q parameters to the simulation mass function, and their jack-knife errors σ_p and σ_q.

4.3 Comparison with the local model

We compare the bias predictions from the mass function fits with the measured local bias from scatter plots, in Fig. 15. Both b_1 and c_2 are shown as a function of halo mass, and for both redshifts that we are studying. We find that, generically, the predicted linear bias b_1 falls below the local bias. This happens for all three mass thresholds we use to fit the mass function. [3]

The best agreement between the linear local bias and the predictions is when the mass function is fitted for masses above $10^{14} M_\odot$. The lower the mass threshold to fit the mass function the worst the agreement between measurements and predictions. For a threshold of $M > 10^{13} M_\odot$ predictions are completely misplaced, for a threshold of $M > 10^{13.5} M_\odot$ we have differences of about 5-10%, while if the threshold is $M > 10^{14} M_\odot$ differences are of few percent. This few percent agreement however have to be taken with caution because we are using the high mass halo tail to predict the bias of a halo sample in which most of the halos had not contributed to the ST fit.

In the same Fig. 15, for comparison with most ST plots in the literature, we have shown also the predictions for the fiducial ST case of $p = 0.3$ and $q = 0.75$. Its performance is similar to the one with a threshold of $10^{13.5} M_\odot$, i.e, with differences about 5-10% with the local bias measurement. If we where to use the values $p = 0.3$ and $q = 0.707$ that also exist in the literature it would yield much lower values of b_1, thus we confirm the convenience of using higher values for q as suggested in Sheth and Tormen (2001).

We show the c_2 values from the scatter plot (black dots with errorbars) in the bottom plot of Fig. 15, against the ST predictions from the mass function fit (dashed lines). As expected c_2 errors from the scatter plot are larger than errors in b_1 since it is more difficult to fit the second order of the Taylor expansion than the first one. For the predictions, statistical errors have been computed using Jack-Knife subsampling (also for b_1) but they are not shown because they are much smaller than the systematics we see by changing the mass threshold.

[3] The only exceptions are halos above $7 \cdot 10^{13} M_\odot$ at $z = 0.5$, where predictions seems to be above measurements. This is because at these masses convergence in the biasing parameters as a function of R_s (i.e., in Fig.2) has not been reached for $R_s = 30$. For this halos, we have checked that if we use a higher smoothing radius (i.e, $R_s = 60$ Mpc/h) we recover the general trend where b_1 measure in the scatter plot is above ones from the mass function.

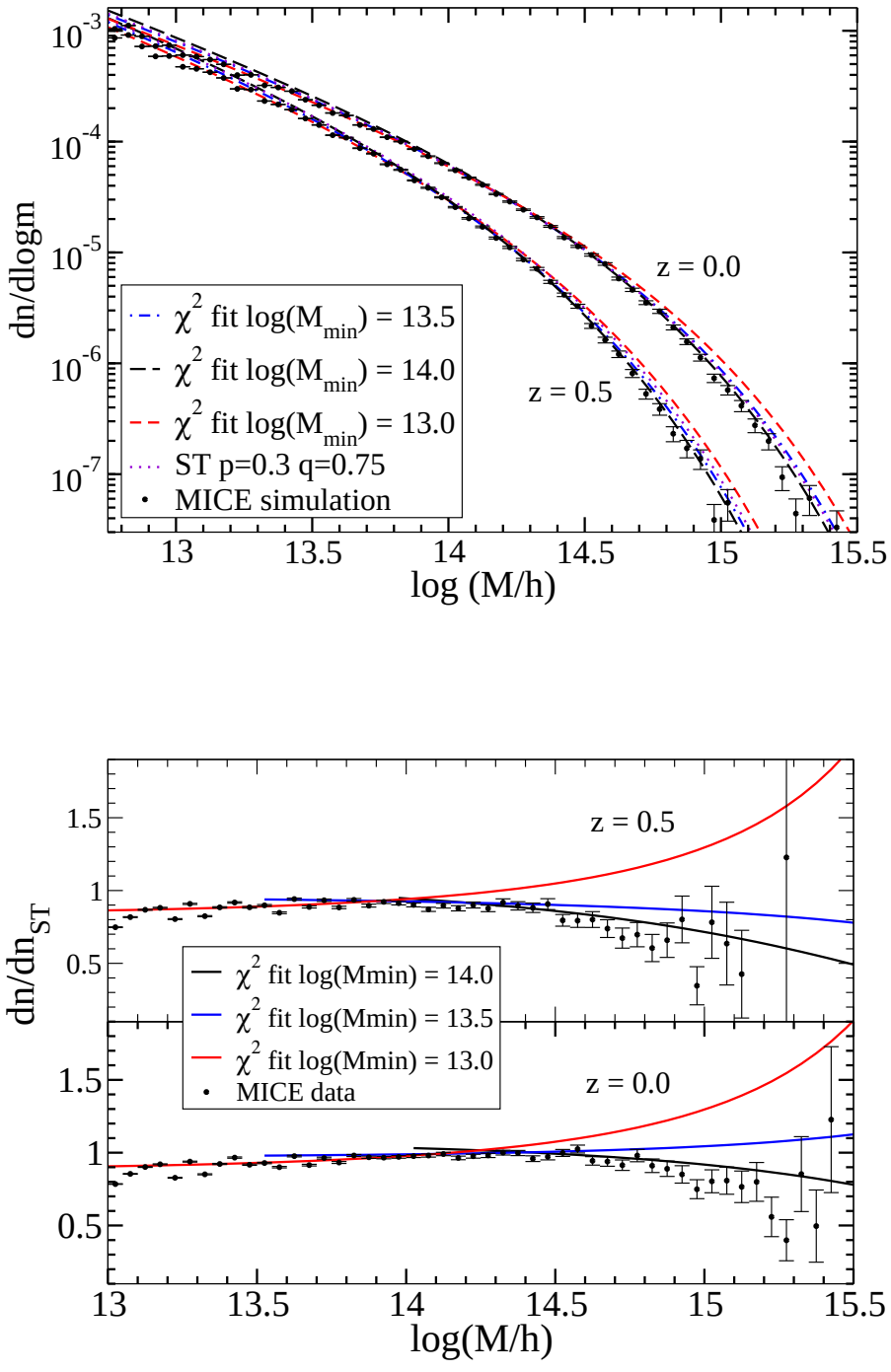

Figure 14. TOP: Mass function for halos in the MICE simulation at redshifts $z = 0$ (upper curves) and $z = 0.5$ lower curves. Compare them with ST best fits starting at $log(M) = 13.0$,13.5 and 14.0. **BOTTOM:** Ratios of the MICE mass function fits and data respect Sheth and Thormen mass function with $p = 0.3$ and $q = 0.75$.

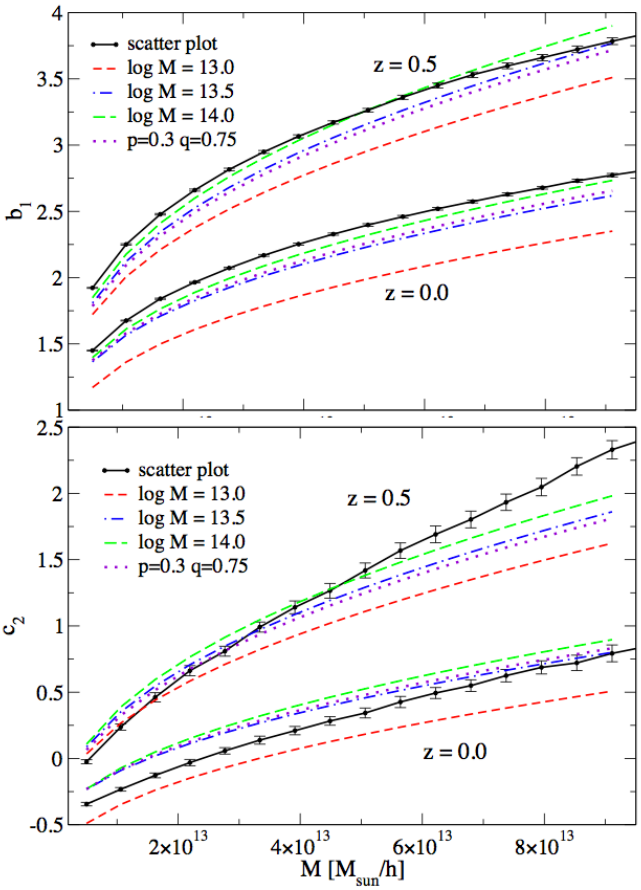

Figure 15. Variation of b_1 (top panel) and c_2 (bottom panel) as a function of the halos mass. In black we show the values measured directly from the δ_h-δ_m local relation in the simulation with a smoothing of $R = 30Mpc/h$ and compare them with ST predictions (dashed lines) and the fiducial ST p=0.3 q=0.75 case (dots). As labeled in the figure each panel have both $z = 0$ and $z = 0.5$ results.

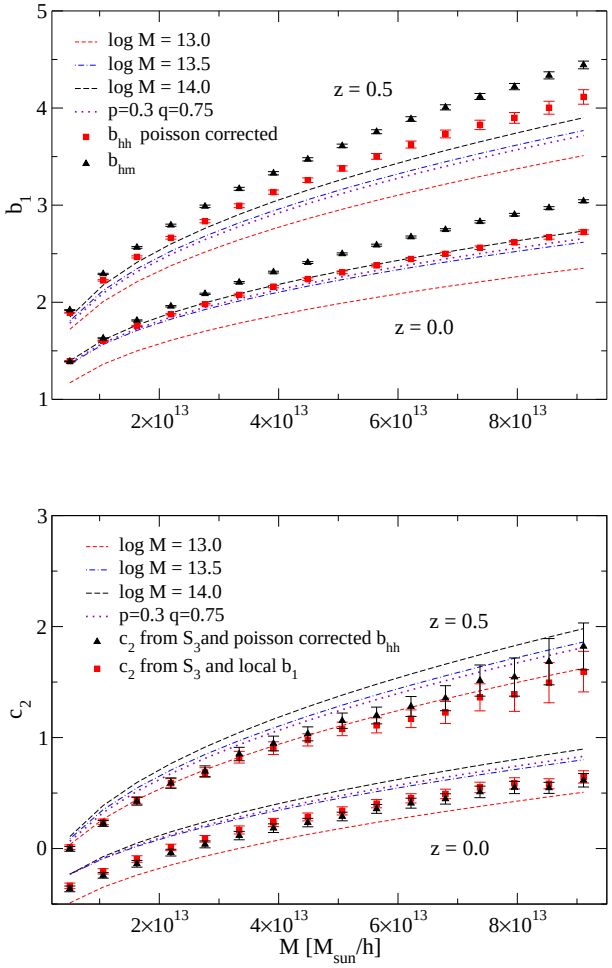

Figure 16. Comparison of the linear and second order bias from clustering with that of ST predictions from the mass function fit. Errors are from Jack-knife method with 64 regions. Smoothing radius of $R = 30Mpc/h$

4.4 Comparison with clustering

So far we have compared the scatter plot bias values both with bias from clustering statistics (section 3) and with ST predictions (this section). This comparisons have allowed the study of the local bias model. Since the local bias is not a direct observable in observations we now proceed to compare directly the bias predictions from the mass function with the bias from clustering. This comparison for b_1 and c_2 is shown in Fig. 16. For reference we have also included the fiducial ST prediction with $p = 0.3$ and $q = 0.75$

We find that the clustering of both b_{hm} and b_{hh} are slightly higher than the ST predictions. Recall that we have shown that the Poisson shot-noise correction does not work for b_{hh}. The correct shot-noise correction is smaller, see Eq.19, and produces values of b_{hh} that are close to b_{hm} Thus the apparent agreement between b_{hh} and the mass function predictions for $z = 0$ is just a fluke and one should only compare to b_{hm} which is not affected by shot-noise. The values of c_2 are also affected by the shot-noise correction.

Similar differences between predictions and measurements where found by Manera et al. (2010) when studying the large scale bias from other set of simulations. If we are looking only at the b_{hh}, ST predictions work at 5-10% level at $z = 0.5$ As we will comment in section §4.5 this could be enough to calibrate mass of halos at about the same percent level. For greater precision more elaborate modeling is needed.

4.5 Halo mass estimation

We now explore the potential use of linear bias b measurements to calibrate the mass threshold of a halos sample. For a given mass-bias (b-M) relation in the halo model (i.e., Eq.24) we can use the measurements of bias b in the halo sample to predict the corresponding mass threshold. This is illustrated in Fig.17. We have used the clustering biases mea-

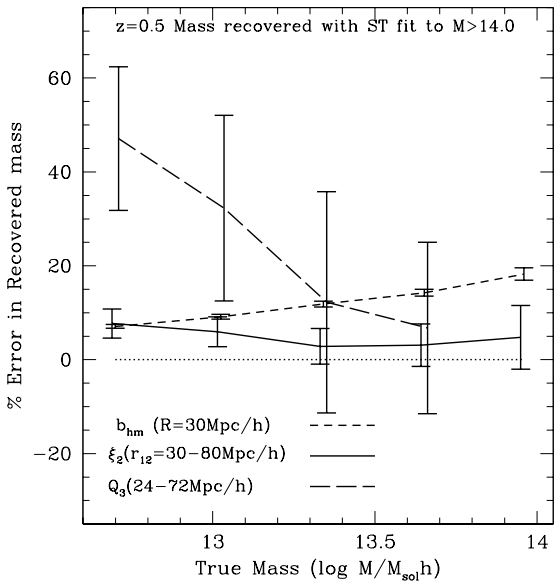

Figure 17. Relative error in the Mass recovered using bias measurements from clustering together with the bias-Mass relation in the peak-background split model obtained from ST fit to MF for $logM > 14$. Short-dashed line corresponds to the bias from the cross-variance b_{hm} in section §2.5. Continuous line correspond to the bias from the 2-point function on large 30-80 Mpc/h scales. Long dashed line come from Q_3 in section §2.3.

sured in the 2-point function (i.e., Fig.5) and in the variance (i.e., Fig.8) at z=0.5 and use the mass-bias relation from the the ST fit to $logM > 14$ (which seems to provide the best fit to data) to calibrate the mass from bias. For the variance we use b_{hm} (the halo-mass cross variance) rather than b_{hh} to avoid discreteness effects.

The idea of recovering the mass function from bias and variance measurements, and subsequently fit for cosmological parameters, have been explored by Lima and Hu (2004, 2005, 2007) in the so-called self calibration method. They assume a peak background split prediction to relate the bias to the mass function (in particular Eq.24 with the fiducial ST values), and allow for an scatter relation between the proxy of the mass (eg. X-ray Temperature) and the true mass. Fig. 17 clearly shows that there is a bias in the recovered mass, which will propagate into the cosmological fits as a systematic error. This bias in the recovered mass, could in principle be corrected with the use of mock samples or the non-linear corrections presented above.

To measure the bias based on the 2-point statistics we need to know σ_8. Otherwise we just recover the value of M in units of σ_8. This is not the case for Q_3, which provides M with independence of σ_8, but at the expense of a larger errorbar and more systematic effects for small masses. For large masses there are too few halos to have a reliable measurement of Q_3. Also note that observations are in redshift space while here we have only show results in real space. We expect differences in redshift space and we defer this to future studies.

5 CONCLUSIONS

In this paper we have used a cosmological dark matter simulation of volume $V = (1536Mpc/h)^3$ from the MICE simulation team to study the halo clustering and bias of halos above $2 \cdot 10^{13} M_\odot$. We have focused in clustering in configuration space (as oppose to Fourier space): the 2 and 3-point correlation function, the variance and skewness and the halo-mass cross-correlations. Our main results can be summarized as follows:

- We have looked at the local deterministic biasing prescription, which assumes a local non-linear relation $T = f(\delta)$ between mass fluctuations, δ, and its tracer,T. In simulations this relation is an approximation with significant scatter around the mean $f(\delta)$ relation. We have fitted this scattered relation with a parabola and found the linear bias b_1 and the quadratic bias, b_2 (or equivalently $c_2 = b_2/b_1$) at different smoothing scales (see Figs 1 & 2). We show that constant biasing values are reached for smoothings larger than $30 - 60Mpc/h$. This provides a new interpretation for the so-called local model: it local only on average over very large scales. This has an immediate application for bias calculations as one can set $R_s \to \infty$ in practice and neglect many of the next to leading order terms in a multipoint expansion.
- We have measured the correlation function of halos, $\xi_h(r)$, and compared it to the matter correlation function, finding that the bias is approximately constant at scales larger than 20Mpc/h (see Figs 2-3) as predicted by the local bias model. Given our errors, there is some room for a small (few percent) scale dependence at scales near the BAO. We have shown (see Fig. 5) that this bias in the correlation is very well matched by the local bias prediction from the scattered δ_m-δ_h parabola, when we use a large smoothing R_s (where convergence to constant values is reached)
- We have measured the 3-point correlation function of halos and fitted its shape to obtain b_1 and $c_2 = b_2/b_1$. We have shown (see Fig. 7) that the linear bias obtained from the 3-point correlation function does not quite match the bias of the 2-pt correlation function (or the local bias, which are the same within errors) at our lower mass bins: $M < 10^{13} M_\odot/h \simeq 50$ particles. The 3-point predictions for b_1 follow well the qualitative behavior of bias as a function of mass and redshift but there are some systematic (2-sigma) deviations at the lower mass end with good agreement for $M > 10^{13} M_\odot/h$. For $M > 10^{14} M_\odot/h \simeq 500$ particles, error bars start becoming too large to conclude.
- We have measured the bias from the halo cross-variance $b_{hm} =< \delta_h \delta > / < \delta^2 >$ and found that it differs from the local bias at about 10%, or even more for the most massive halos (see Fig. 8). The true local bias can be recovered, if we include non-linear correction (using the measured b_2 of the local model). This is in contrast to the bias from the 2-pt correlation function for which there was no need of including nonlinear terms.
- We have measured the bias from the halo variance $b_{hh}^2 = (< \delta_h^2 > -1/\bar{n}) / < \delta^2 >$ and found that it is different from b_{hm} and from the linear local bias. We have shown that in order to be able to predict b_{hh} from the local bias we need to

take into account *both* nonlinear and stochastic effects (see Fig. 8).

• We have shown that the appropriate discreteness correction to the variance is sub-Poisson, and found that its ratio to the Poisson term $1/n$ is approximately constant in our range of masses. (see Fig. 10). Overcorrecting the variance with $1/n$ masks the nonlinear contributions, thus giving an estimated value of b_1 apparently closer to that of the local bias (specially at z=0), as we show in Fig. 8.

• We have fitted the mass function of halos with a Sheth and Thormen functional form and applied the peak-background split Ansatz to predict the bias parameters. These predictions depend significantly on the mass threshold used to fit the mass function and they give systematically lower linear bias (about 5-10%) than that measured in clustering or local relation (see Fig. 16 and Fig.15).

• Finally, we have estimated the mass of halos from the measured bias (Fig. 17), showing that there is a systematic error when using the common ST peak-background split prediction. These systematic errors have to be taken into account when recovering the mass function from clustering of halos, since they will propagate to the estimator of cosmological parameters, like the dark energy equation of state.

We can conclude from the above that the different bias predictions are only accurate to 5-10% level. In the case of the 2-point functions (auto and cross-correlations), the local model seems accurate and we find that the origin of the discrepancy lies in the peak-background prescription. This is not so clear for the 3-point function, where probably both assumptions contribute to the error. For the smoothed moments, we find that next to leading order and discreetness corrections (to the local model) are needed at the $10-20\%$ level. Although this accuracy might still be adequate for current data, where typical errors are 10-20% (eg. Norberg et al. 2002, Zehavi et al. 2005, Gaztanaga et al. 2005, Nichol et al 2006), more work needs to be done to narrow this to the percent level that will be likely needed in upcoming and future surveys for precision cosmology and better understanding of galaxy evolution.

ACKNOWLEDGMENTS

We thank all the MICE collaboration team, and specially P. Fosalba who provided the central positions of halos in the simulation. We thank Roman Scoccimarro for his comments on the first draft of this paper. The MICE simulations have been developed at the MareNostrum supercomputer (BSC-CNS) thanks to grants AECT-2006-2-0011 through AECT-2010-1-0007. Data products have been stored at the Port d'Informaci Cientfica (PIC). This work was partially supported by NSF AST-0607747, NASA NNG06GH21G and NSF AST-0908241, and the Spanish Ministerio de Ciencia e Innovacion (MICINN), projects AYA2009-13936, Consolider-Ingenio CSD2007- 00060 and research project 2009-SGR-1398 from Generalitat de Catalunya.

REFERENCES

Bardeen J., Bond J., Kaiser N., Szalay A., 1986, Astropy.J., 304,15
Barriga J., Gaztanaga E., 2002, MNRAS 361, 842
Baugh, Gaztanaga & Efstathiou, 1995, MNRAS 274, 1049
Bernardeau F., Colombi S., Gaztanaga E., Scoccimarro R., 2002, Phys. Rep. 367, 1
Brown, M.J.I., Zheng, Z., White, M., Dey, A., Jannuzi, B.T., A. J. Benson, K. Brand, M. Brodwin, D. J. Croton, 2008, ApJ, 682, 937
Cai Y.-C., Bernstein G., Sheth R. K., 2010, arXiv:1007.3500
Catelan, P., Matarrese, S. and Porciani, C., 1998, Astrophys. J. Letters, 502, L1
Casas-Miranda R., Mo H.J. Sheth R.K., Borner G., 2002, MNRAS 333, 730
Cole S., Kaiser N., 1989, MNRAS 237, 1127
Cooray A. & Sheth, 2002, Phys. Rept. 372, 1
Crocce M., & Scoccimarro R., 2008, Phys.Rev.D, 78, 103521, astro-ph 070427
Crocce, M., Fosalba, P., Castander, F. J.; Gaztanaga, E., 2009, Mon.Not.Roy.Astron.Soc., 403,Issue 3, 1353
Dekel, A & Lahav O., 1999, ApJ 520, 22
Cabre, A. % Gaztanaga E., 2009, Mon.Not.Roy.Astron.Soc., 393, 1183
Desjacques V., Crocce M., Scoccimarro R., Sheth R.K., 2010, submitted to PRD, eprint arXiv:1009.3449
Eke, V. R., Cole, S., Frenk, C. S. 1996, MNRAS, 282, 263
Feldman H.A., Frieman J.A., Fry J.N. & Scoccimarro R., 2001, PRL 86, 1434
Fosalba P. & Gaztañaga E. 1998, MNRAS, 301, 503
Fosalba P., Gaztañaga E., Castander F. J., Manera M., 2008, MNRAS, 391, 435
Frieman J.A., & Gaztanaga E., 1994, ApJ 425, 392
Frieman J.A., & Gaztanaga E., 1999, ApJ 521, L83
Fry J.N., 1994, Phys. Rev. Lett. 73, 215
Fry J.N., & Gaztanaga E., 1993, ApJ, 413, 447
Gaztanaga E., 1994, Mon.Not.Roy.Astro.Soc., 268,913
Gaztanaga E. & Frieman, J. A., 1994, ApJ 437, L13
Gaztanaga E., Scoccimarro R., 2005, MNRAS 361, 824
Gaztanaga E., Norberg P., Baugh C.M., Croton D.J., 2005, MNRAS 364, 620
Guo H. & Jing P., 2009, ApJ, 702, 425
Juszkiewicz, R., Bouchet, F.R, & Colombi, S., 1993, Astrophys. J. 412, L9
Lima M. & Hu W. 2007, PRD 76, 123013
Lima M. & Hu W. 2005, PRD 72, 043006
Lima M. & Hu W. 2004, PRD 70, 043504
Manera M. Sheth R.K., Scoccimarro R., 2010, MNRAS 402, 589
Marin F.A., Wechsler R.H., Frieman J.A., Nichol R.C, 2008, ApJ, 672, 849-860
Martino M.C., Sheth R.K., 2009, MNRAS, 394, 2109
Matsubara T., 2008, PhRvD, 78, 083519
Mo H.J., Jing Y.P., White S.D.M., 1997, MNRAS, 284, 189
Nichol, R.C. et al. 2006, MNRAS 368, 1507
Norberg P., et al., 2002, MNRAS, 332, 827
Peebles P.J.E., 1980, The Large-Scale Structure of the Universe. Princeton Univ. Press, Princeton, NJ
Press W. & Schechter P., 1974, Astrophys. J., 304, 297
Sefussati E., Scoccimarro R., 2005, PRD 71, 063001
Sheth R.K., Lemson G., 1999, MNRAS , 304, 767
Sheth R.K. & Tormen G., 1999, MRNAS, 301,119
Sheth R.K. & Tormen G., 2001, MRNAS, 323,1
Scoccimarro R., Couchman H.M.P., & Friedman J.A., 1999, ApJ 517, 531

Scoccimarro R., Sheth. R.K., Hui L., Jain B., 2001, ApJ 546, 20
Seljak U., Hamaus N., Desjacques V., 2009, PhRvL, 103, 091303
Somerville R.S., Lemson G., Sigad Y., Dekel A., Kauffmann G., White S.D.M., 2001, MNRAS, 320, 289
Tegmark, M. & Peebles, 1998, ApJ 500, L79
Tegmark M., Bomley B.C., 1999, ApJ 518, L69
Tinker, J.L., Weinberg, D.H., Zheng, Z., 2006, MNRAS 368, 85
Tinker, J.L. & Wetzel, A.R., 2010, ApJ 719, 88
Tinker J. L., Robertson B. E., Kravtsov A. V., Klypin A., Warren M. S., Yepes G., Gottlober S., 2010, arXiv, arXiv:1001.3162
Verde, L., Heavens, A. F., Percival, W. J., Matarrese, S., Baugh, C. M. et al., 2002, MNRAS, 335, 432
Warren M.S., Abazajiian K., Holz D.E., Teodoro L., 2006, ApJ, 646, 881
Zheng, Z., Berlind, A.A., Weinberg, D.H., 2005, ApJ, 633, 791
Zheng, Z., Zehavi, I., Eisenstein, D.J., Weinberg, D.H., Jing, Y.P., 2009, ApJ, 707, 554
Zehavi I., et al., 2005, ApJ, 630, 1